

Simulation of a Bioreactor with an Improved Fermentation Kinetics – Fluid Flow Model

Emily Liew Wan Teng¹ and Law Ming Chiat^{2*}

¹Department of Chemical Engineering, Faculty of Engineering and Sciences, Curtin University, Sarawak Campus, CDT 250, 98009 Miri, Sarawak, Malaysia

²Department of Mechanical Engineering, Faculty of Engineering and Sciences, Curtin University, Sarawak Campus, CDT 250, 98009 Miri, Sarawak, Malaysia

ABSTRACT

Ethanol fermentation experiments were carried out using a stirred tank equipped with a Rushton turbine. The data were used to estimate kinetic parameters based on a newly developed kinetics model originated from Herbert's microbial kinetics model. This newly developed model took into account the effects of aeration rate (AR) and stirrer speed (SS). Experiment data i.e. glucose, ethanol and biomass concentrations obtained from different experiment sets were used for kinetics prediction. Assuming a perfectly-stirred condition, the kinetic parameters were initially estimated through solving Herbert's model equations. These estimated kinetic parameters were then incorporated in a Computational Fluid Dynamics (CFD) model but the simulation results did not agree well with the experiment findings. Based on the proposed CFD model, the kinetic parameters were corrected. The correction factors were expressed as functions of AR and SS . This analysis highlighted the need to estimate kinetic parameters based on CFD simulation because it is able to account for the spatial variation in a reactor. A sensitivity analysis of the kinetic parameters using the coupled CFD-fermentation kinetic model was carried out to further understand the influence of each set of kinetic parameters on the model prediction. It was found that the sensitivities of the kinetic parameters varied with the concentrations of glucose, ethanol and biomass.

Keywords: Bioreactor, CFD, ethanol, fermentation, kinetics, Rushton turbine

Article history:

Received: 14 October 2014

Accepted: 14 April 2015

E-mail addresses:

emily2703@gmail.com (Emily Liew Wan Teng),

m.c.law@curtin.edu.my (Law Ming Chiat)

*Corresponding author

INTRODUCTION

Bioreactors are most widely used in chemical and bioprocess industries such as fermentation, for mixing and combining liquids for biochemical reactions (Harvey & Rogers, 1996). It is vital to ensure that the requirements of the microbial environment were met for maximum microbial growth, such as temperature, pH and oxygen content

(Hutmacher & Singh, 2008). As a result, the bioreactor performance is complex due to the complicated interrelations between the microbial cells and the governing environment. The exact description of flow movement by a simple model is not possible as the flow caused by the impeller embedded in the bioreactor is overlapped by turbulence fluctuations.

Another main issue to be addressed is the kinetics of ethanolic fermentation. It is evident that an ideally mixed assumption is inadequate to describe the wide range of length scales present in stirred tanks (Fox, 1998). Thus, it is vital to employ micro-mixing behaviour for a stirred tank. So far, most kinetics is limited to macro-kinetics i.e. the interactions of the microenvironment around the microbial cells with its dependency on the biological reaction are not taken into account. The metabolism of microorganisms is very complex, whereby the metabolism varies during the cycle of cell growth and replication. These phenomena cause inhomogeneity of the microorganism population. There might be morphological differentiation of microbial cells accompanied by changes in the cell metabolisms. Thus, what is observed is only an averaged behaviour over the great number of cells in different states. It is tough to establish a very detailed model to describe all the microbial metabolic activities. One of the ways suggested is the consideration of aeration rate (AR) and stirrer speed (SS) as manipulated variables in the bioreactor system. According to García-Ochoa and Gomez (2009), the most important operating conditions in a stirred tank bioreactor are AR and SS . This is due to the fact that in a stirred tank bioreactor, high values of mass and heat transfer rates are attained. Oxygen mass transfer is influenced by both AR and SS (García-Ochoa *et al.*, 1995). Both AR and SS offer more effects via the mixing mechanism of a stirred tank bioreactor compared to other operating conditions as both affect the mass, heat and oxygen transfer throughout the bioreactor operation and provide turbulence in the bioreactor.

Starzak *et al.* (1994) summarised a list of kinetic models that were used to simulate the kinetic ethanolic fermentation process. These kinetic models consist of a set of ordinary differential equations (ODE), which describe the material balance of biomass, product (ethanol) and substrate (glucose). Optimisation techniques were used to obtain the model constants by minimising the error between the kinetic models and experiment data. All these approaches assumed perfectly mixed behavior, which neglects the spatial variation of the fermentation process. Spatial variation of the fermentation process is defined as the variation throughout the bioreactor tank that is associated with microorganism population.

In order to analyse the highly complex fluid flow in mechanically stirred reactors, computational fluid dynamics (CFD) offers a potentially useful tool for this purpose. In recent years, CFD has been used intensively in the simulation of single-phase and multiphase flow within relatively simple geometries, whereby simulation results are to be compared with experiment data (Kuipers & van Swaaij, 1998). Nevertheless, there are only a few CFD simulations that coupled fluid flow and fermentation in the models. This is due to large-time scale difference between fluid flow and its reactions. Consequently, CFD simulation of fermentation process is too time-consuming. Van Zyl (2012) developed a three-dimensional (3-D) CFD model with the incorporation of fermentation reactions. However, the reaction terms were not strongly coupled with the fluid flow physics and the CFD results were not compared with the experiment data. In addition, there were also a number of CFD-reaction models but these were on different reactions such as gluconic acid (Elqotbi *et al.*, 2013) and

polymerisation processes (Patel *et al.*, 2010; Roudsari *et al.*, 2013). To avoid an excessive computing effort, Bezzo and Macchietto (2004) proposed a hybrid multizonal/CFD approach to the model bioreactor. The computational domain was divided into 20 zones and a perfectly-stirred reactor model was assumed in each zone. Liew *et al.* (2013) simulated a CFD with fermentation reaction; however, since it was a steady-state model, it is impossible to assess the accuracy of the simulation with experiment data as a function of time.

The objectives of this study were: (a) to carry out an experimental study on *AR* and *SS* on biomass, substrate (glucose) and product (ethanol) concentrations in a mechanically-stirred tank bioreactor; (b) to determine the kinetic parameters of the fermentation process using a perfectly-stirred reactor model and experiment data from (a); (c) to incorporate the kinetic parameters obtained in (b) with a simplified time-dependent CFD model that does not require much computational time, and (d) to conduct CFD simulations for the prediction of the bioreactor performance, in terms of ethanol production in the gas-liquid mechanically-stirred bioreactor and validation with experiment results obtained in (a).

MATERIALS AND METHODS

The schematic diagram of the experiment setup is shown in Fig.1. Experiments were carried out in a 2L elliptical-bottom shaped cylindrical tank of internal diameter of 0.128m that was transparent to light. A six-bladed Rushton turbine impeller of diameter 0.044m was utilised for this experimental study. Glucose was utilised as the main substrate for the fermentation medium. Air was admitted to the bioreactor using a cylindrical sparger located at the bottom of the tank, beneath the impeller. Agitation was carried out using a variable speed DC motor. The speed ranged from 30 to 1,100 rpm for the 2L bioreactor tank specification. The DC motor drive was a maintenance free, 150W quiet, direct motor-driven operation.

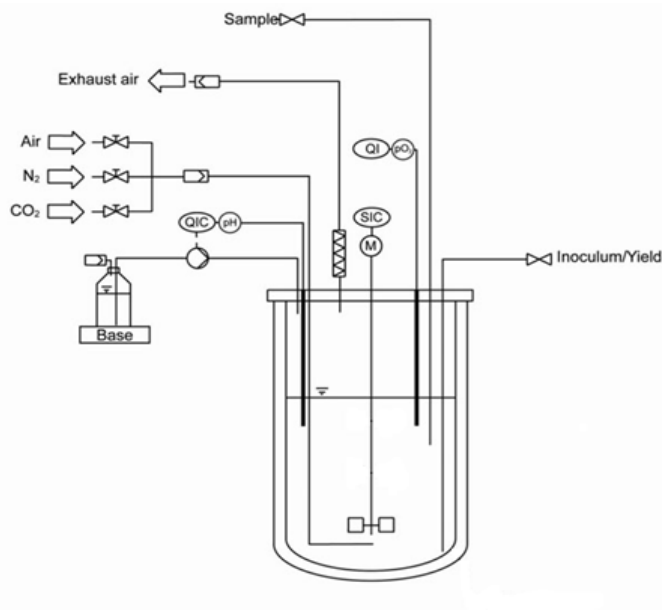


Fig.1: Schematic diagram of experiment setup used for this study.

Microorganism and Inoculum

Experiments were conducted using a BIOSTAT A-plus 2L, MO-Assembly bioreactor operated in batch mode. This bioreactor was a solid, autoclavable laboratory bioreactor system that was suitable for a wide range of research and industrial applications. It was applicable for microbial culture for the growth of bacteria, yeast and fungi as well as cell culture for the growth of animal, insect and plant cells.

A Rushton turbine was utilised to study the effect of agitation, whereas an air sparger was utilised to study the effect of aeration. Commonly used for efficient mixing and maximum oxygen transfer within the bioreactor, the Rushton turbine is a disc turbine that was used in many fermentation processes for fast air stream break-up without itself becoming flooded in air bubbles (Stanbury & Whitaker, 1995).

On the other hand, 40 mL of inoculum was prepared in a conical flask and was incubated at 28 °C for 8 hours. The microorganism used in this study was *Saccharomyces cerevisiae*, which is the most commonly used microorganism in fermentation processes (Schugerl & Bellgardt, 2000). *Saccharomyces cerevisiae* was purchased in ready-made powder form from Sigma Aldrich. Thus, there was no isolation and screening of the microorganisms. *Saccharomyces cerevisiae* was directly added into the inoculum for growth to occur, and the pH was adjusted to pH 5 for optimum growth. It was vital that the inoculum was prepared in a contamination-free environment due to its physiological condition, which had a major effect on fermentation. Therefore, the conical flask was sterilised before usage to avoid any contamination. Steam was utilised for sterilisation and was applied at 15 psi. The inoculum was prepared based on the formulation by Thatipamala *et al.* (1992), which is outlined in Table 1, along with an addition of 1 g of Baker's yeast. Baker's yeast was added after the inoculum was autoclaved. The inoculum was then incubated for 8 hours.

TABLE 1 : Inoculum Preparation Formulation

Constituents	Amount (g/L)
Glucose	50
Yeast extract	5.0
NH ₄ Cl	2.5
Na ₂ HPO ₄	2.91
KH ₂ PO ₄	3.0
MgSO ₄	0.25
CaCl ₂	0.08
Citric acid	4.3
Sodium citrate	3.0

Fermentation Medium

The composition of the fermentation medium was also prepared by Thatipamala *et al.* (1992). 1.5 L of the fermentation medium was prepared in the bioreactor tank by adding the constituents listed in Table 1 that were similar to the inoculum preparation formulation, without the addition

of Baker's yeast. The fermentation medium was then sterilised under 121 °C for 20 mins and allowed to cool down under room temperature at 30 °C. After 4 hours, the freshly prepared 40 mL of inoculum was added to the cooled fermentation medium and mixed thoroughly.

Operating Conditions

Once the fermentation medium had been mixed, the pH of the medium was measured and subsequently adjusted to pH 5 with the addition of acid (sulphuric acid) or alkali (sodium hydroxide). The temperature was adjusted to 30 °C and maintained with the utilisation of a temperature controller, which was embedded in the bioreactor. *AR* and *SS* were set according to the preferred conditions, respectively.

The fermentation process was started after all these operating conditions were maintained at the desired settings. Samples taken at sampling intervals of 2 to 4 hours were analysed for glucose and ethanol concentrations immediately after the samples were extracted from the bioreactor. The experiments were repeated at various conditions of *AR* and *SS* within the range of 1.0-1.5LPM of *AR* and 100-150rpm of *SS*. The operating ranges of *AR* (1.0LPM-1.5LPM) and *SS* (100-150rpm) were selected for this study as a preliminary study for the improved kinetics model. The operating ranges for both *AR* and *SS* were not within a large range as it would be easier to analyse the possibility of both parameters in future studies. Should the effects of both parameters in the improved kinetics model be low, the range would be increased in future studies.

Bioreactor Operating Cycle

The bioreactor was ready for operation once the inoculum and fermentation mediums were ready. The bioreactor was connected to a computer that was fully automated with control systems, with operating parameters such as pH, temperature, oxygen content, *AR* and *SS* that could be controlled automatically. Once all operating parameters were set based on the desired conditions, the fermentation process began, and the operating parameters were recorded in the computer throughout the fermentation process. Samples were extracted during the fermentation process every 2 hours; sampling was stopped once the fermentation process was completed after 45 hours.

Analytical Procedures

After the samples were extracted from the bioreactor, the samples were first filtered and then analysed for the concentrations of glucose and ethanol concentrations, as well as optical density. Glucose and ethanol concentrations were analysed using R-Biopharm test kits and UV spectrophotometer under a wavelength of 340 nm, as outlined in the procedures manual provided by the test kits. The UV spectrophotometer utilised was Perkin Elmer Lambda 25 UV/Vis Systems with a range between 190 and 1,100 nm (with a fixed bandwidth of 1 nm). However, for the analysis of optical density, no test kits were required as the UV spectrophotometer could directly analyse the optical density measurements. All samples were tested under room temperature for consistency. Optical density was measured to observe the microorganisms'

growth throughout the fermentation process. The optical density decreased subsequently with fermentation time. Once the optical density decreased steadily, the results indicated that the fermentation process was completed as the microorganisms' growth had halted.

Modelling

Assumptions. It is expensive to simulate a complete three-dimensional (3-D) model of the bioreactor. To reduce the computational time, a two-dimensional (2-D) model was developed. In addition, air was not accounted for in the 2-D model due to its small volume fraction in the bioreactor. To verify this assumption, a 3-D CFD model of the bioreactor (without reaction) was simulated using commercial software STAR-CCM+ (version 8.04, CD-adapco, UK) and it was found that average volume fraction of air was about 0.8%, as shown in Fig.2. In addition, the oxygen consumption rate was not calculated in the model. Consequently, the gas phase was not considered. Nevertheless, the effect of the oxygen was accounted implicitly throughout the kinetic scheme discussed in the later section.

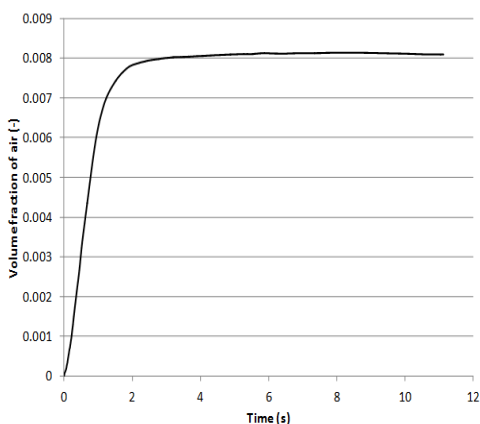


Fig.2: The average volume fraction of air simulated by a 3-D CFD model.

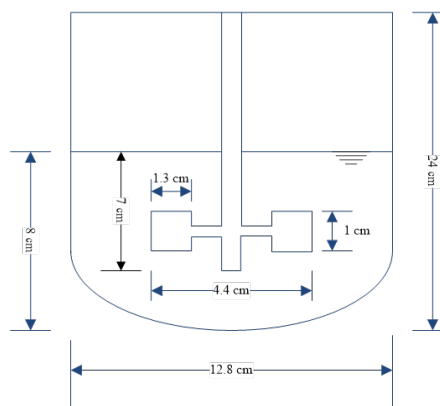


Fig.3: Geometry of the bioreactor.

Model description. Generally, a CFD analysis often involves a number of procedures. Firstly, a computational domain of the problem under investigation has to be identified. After that, a set of governing equations that describe the physics of the phenomenon has to be determined. These governing equations are often presented in the form of partial differential and algebraic equations. The initial input and boundary conditions for the governing equations are required in order to obtain a unique solution for the CFD analysis. The following section describes the methodology used in the CFD analysis of this current work.

Computational domain. The dimensions of the stirred tank are shown in Fig.3. However, due to the symmetry of the tank, only half of the bioreactor tank was simulated in this current study.

Governing transport equations. To calculate the liquid velocity in the bioreactor, Navier-Stokes equations were required to be solved. These equations consist of mass and momentum conservation equations. The equations were required to be solved simultaneously as they are

coupled. As the experiment was carried out at isothermal condition, the density change was negligible. The specific temperature used in this study was room temperature at 30 °C. Thus, incompressible flow was assumed. The mass conservation equation for the incompressible bioreactor solution can be expressed as:

$$\rho \nabla \cdot \mathbf{u} = 0 \quad [1]$$

where ρ is the density of the bioreactor solution, \mathbf{u} is the velocity vector and ∇ is the divergence operator (Versteeg & Malalasekera, 2007).

On the other hand, since the liquid density was significant ($\rho \approx 1023 \text{ kg/m}^3$), the volume force due to the liquid mixture, $\rho \mathbf{g}$, was accounted for in the momentum conservation equation, which is expressed as:

$$\rho \frac{\partial \mathbf{u}}{\partial t} + \rho (\mathbf{u} \cdot \nabla) \mathbf{u} = \nabla \cdot \left[-\rho \mathbf{I} + (\mu + \mu_T) (\nabla \mathbf{u} + (\nabla \mathbf{u})^T) - \frac{2}{3} \rho k \mathbf{I} \right] - \rho \mathbf{g} \quad [2]$$

where ρ is the liquid pressure; μ is the liquid dynamic viscosity; μ_T is the turbulent viscosity and k is the turbulent kinetic energy.

The bioreactor normally operates in turbulent regime ($\text{Re} \approx 40,000$) so the turbulent phenomenon has to be accounted for by solving the $k - \varepsilon$ equations. The turbulent kinetic energy, k can be calculated as:

$$\rho \frac{\partial k}{\partial t} + \rho (\mathbf{u} \cdot \nabla) k = \nabla \cdot \left[\left(\mu + \frac{\mu_T}{\sigma_k} \right) \nabla k \right] + P_k - \rho \varepsilon \quad [3]$$

On the other hand, the turbulent dissipation rate, ε was obtained as follows:

$$\rho \frac{\partial \varepsilon}{\partial t} + \rho (\mathbf{u} \cdot \nabla) \varepsilon = \nabla \cdot \left[\left(\mu + \frac{\mu_T}{\sigma_\varepsilon} \right) \nabla \varepsilon \right] + C_{\varepsilon 1} \frac{\varepsilon}{k} P_k - C_{\varepsilon 2} \rho \frac{\varepsilon^2}{k} \quad [4]$$

where $\mu_T = \rho C_\mu \frac{k^2}{\varepsilon}$, P_k is the turbulent kinetic energy production rate, $P_k = \mu_T + [\nabla \mathbf{u} : (\nabla \mathbf{u} + (\nabla \mathbf{u})^T) - \frac{2}{3} \rho k \mathbf{I}]$. The values for various coefficients are $C_\mu = 0.09$, $C_{\varepsilon 1} = 1.44$, $C_{\varepsilon 2} = 1.92$, $\sigma_k = 1.0$ and $\sigma_\varepsilon = 1.3$. These numerical values are based on curve-fitting of comprehensive turbulent flow data (Versteeg & Malalasekera, 2007).

The medium contained four main components i.e. water as well as glucose, ethanol and biomass concentrations. Since water was present in excessive amount, the remaining components were modelled as diluted species. Thus, the concentration of a component in the solution can be calculated by the following transport equation:

$$\frac{\partial c_i}{\partial t} + \mathbf{u} \cdot \nabla c_i = \nabla \cdot (D_i \nabla c_i) + R_i \quad [5]$$

where D_i is the diffusion coefficient of the component i ($i = \text{substrate, product, biomass}$) and is the corresponding reaction rate. The reaction rate of each of these components is discussed in Section 3.3.

Boundary conditions and solution procedure. Wall function based on the logarithmic wall law (Kuzmin *et al.*, 2007) was used at the bioreactor tank wall while the slip boundary condition was used for the liquid surface for $k - \varepsilon$ model. The rotational speed, μ_θ , is defined at the impeller wall by:

$$u_\theta = r\omega \quad [6]$$

where r is the radial distance from the centre of the tank and ω is the angular velocity.

As for the species equation, zero normal gradient is implemented at the liquid surface:

$$-\mathbf{n} \cdot D_i \nabla c_i = 0 \quad [7]$$

where \mathbf{n} is the outward normal vector at the boundary.

At the bioreactor walls, no flux condition was prescribed:

$$-\mathbf{n} \cdot (-D_i \nabla c_i + \mathbf{u}c_i) = 0 \quad [8]$$

The governing equations [1] - [8] were solved using COMSOL Multiphysics v4.1 (COMSOL, Sweden). The computational domain was meshed using 4886, 11222, 26416 elements. No appreciable difference was observed for the cases with 11222 and 26416 elements. The simulations were carried out using 26416 elements. It takes approximately 2 hours for a simulation to be completed over a 45-hour fermentation process. The model also avoids the need to simulate a three-dimensional two-phase flow model, which requires a simulation time of approximately 1 week.

Reaction kinetics of the fermentation process. In this study, the hydrodynamics of liquid-gas flows in a mechanically-stirred bioreactor tank was simulated using Herbert's concept of endogenous metabolism. This kinetics concept has been used in numerous studies to describe the kinetics of ethanolic fermentation with sufficient accuracy (Starzak *et al.*, 1994). Studies on the impacts of AR and SS were focused on the concentration profiles of biomass (X), substrate (glucose) (S) and product (ethanol) (P) in terms of product yield and productivity.

In the kinetics hybrid model development, experiment data of X , S and P concentrations for different conditions of AR and SS were used to predict the kinetics parameters, $k_1, k_2, k_3, \dots, k_6$ using Herbert's concept. The range of AR was set to be in the range from 1.0-1.5LPM and SS from 100-150rpm, which is similar to the experiment range. For this purpose, Herbert's concept was applied as follows: It is assumed that the observed rate of biomass formation comprised the growth rate and the rate of endogenous metabolism, which are known as Herbert's microbial kinetics model (Starzak *et al.*, 1994):

$$\begin{aligned} R_x &= (R_x)_{growth} + (R_x)_{end} \\ &= \left(\frac{k_1 SX}{k_2 + S} \exp(-k_3 P) - k_6 X \right) / 3600 \end{aligned} \quad [9]$$

where $-k_6 X$ is the rate of growth due to endogenous metabolism by a linear dependence. The division of a constant of 3600 is to convert the reaction rate from $\text{kg}/(\text{m}^3\text{hr})$ to $\text{kg}/(\text{m}^3\text{s})$.

It was also assumed that the rates of substrate consumption and product formation were proportional to the biomass growth rate:

$$R_s = \left(-k_3 \frac{k_1 SX}{k_2 + S} \exp(-k_5 P) \right) / 3600 \quad [10]$$

$$R_p = \left(k_4 \frac{k_1 SX}{k_2 + S} \exp(-k_5 P) \right) / 3600 \quad [11]$$

Kinetic parameters based on perfectly-stirred bioreactor assumption. The kinetic parameters' estimation was obtained by minimising the errors between the experiment data and the model equations. The model formulation consisted of equations [9]-[11], which implied a perfectly-stirred tank condition (Liew *et al.*, 2013). MATLAB v2006 (The MathWorks, Inc, US) was utilised to predict the values of μ . Any set of experiment data within the experiment range was utilised for prediction. The experiment data was first arranged in a spreadsheet and imported into MATLAB. All initial values of substrate concentration, product concentration and biomass concentration (based on experiment data), along with the AR and SS conditions, were clearly stated in MATLAB before the prediction began. Next, initial values of k_1 to k_6 were provided as well. Any initial values of k_1 to k_6 could be assumed since the values of μ would change based on different sets of experiment data provided. The initial k_1 to k_6 values could be changed after the first prediction if the values were not satisfied. ODE45 was selected as the solver for the prediction as it was the most common solver used for prediction purposes.

Next, iterations were performed to predict the values of k_1 to k_6 by utilising the solver selected. During iterations, the solver would fit the experiment data with the kinetic model embedded with the kinetics from k_1 to k_6 . Iterations would stop once the values of k_1 to k_6 were predicted. The values of k_1 to k_6 were considered acceptable if the exit flag value were positive, where an exit flag was an integer that showed that iterations had been halted and completed. Positive exit flags correspond to successful outcomes whereas negative exit flags correspond to failure outcomes. Based on the assumptions proposed in this study, the total number of iterations used in ODE45 to obtain the positive and negative exit flags were approximately 1,500 and 500, respectively.

In order to check and compare the fitness of the kinetics with respect to the experiment data, plots of model fitting with respect to the experiment data were generated. In the case of unsatisfied fitness, initial values of k_1 to k_6 can be reassumed for new predictions of k_1 to k_6 values. Iterations can be done again for new predictions.

Improved kinetic parameters for CFD analysis. It was discovered that when the equation [9]-[11] were coupled with the CFD model (equations [1]-[8]), the kinetic parameters obtained from Section 3.3.1 were found to over-estimate the fermentation reaction. Hence, correction factors were introduced to the rate expressions i.e. [9]-[11]. These corrected expressions, denoted by a subscript, *C*, are shown as follows:

$$R_{x,c} = \left(\alpha_1 \frac{k_1 SX}{k_2 + S} \exp(-\alpha_5 k_5 P) - \alpha_6 k_6 X \right) / 3600 \tag{12}$$

$$R_{s,c} = \left(-\alpha_3 k_3 \frac{k_1 SX}{k_2 + S} \exp(-\alpha_5 k_5 P) \right) / 3600 \tag{13}$$

$$R_{p,c} = \left(\alpha_4 k_4 \frac{k_1 SX}{k_2 + S} \exp(-\alpha_5 k_5 P) \right) / 3600 \tag{14}$$

Each correction factor, *i*, α_i was modelled using a second-order spline, which is defined as:

$$\beta_0 + \beta_1 X_1 + \beta_2 X_2 + \beta_3 X_1 X_2 + \beta_4 X_1^2 + \beta_5 X_2^2 \tag{15}$$

where $X_1 = AR - 2$ and $X_2 = \frac{(SS - 225)}{75}$

The expressions of the kinetic parameters, k_1, \dots, k_6 and the correction factors $\alpha_1, \dots, \alpha_6$ are listed in Table 2.

TABLE 2 : Expressions of the Kinetic Parameters and Correction Factors

$k_1 = (1.3998 - 0.2852X_1 + 0.3692X_2) \left[\frac{\text{g}}{\text{L.hr}} \right]$	$\alpha_1 = 3.3324 + 1.4669X_1 - 0.2010X_2 + 5.8336X_1X_2 - 4.7719X_1^2 - 2.1244X_2^2$
$k_2 = 0.01 \left[\frac{\text{g}}{\text{L}} \right]$	$\alpha_2 = 1$
$k_3 = (0.5377 - 0.0148X_1 + 0.022X_2) [-]$	$\alpha_3 = 13.6026 + 13.2693X_1 + 8.3081X_2 + 7.0327X_1X_2 + 1.9638X_1^2 + 0.4782X_2^2$
$k_4 = (0.0738 + 0.0142X_1 + 0.0128X_2) [-]$	$\alpha_4 = 6.9135 + 1.0897X_1 - 0.6332X_2 + 13.5979X_1X_2 - 11.719X_1^2 - 5.336X_2^2$
$k_5 = (0.8072 - 0.1019X_1 - 0.0211X_2) \left[\frac{\text{L}}{\text{g}} \right]$	$\alpha_5 = 0.8171 + 0.3420X_1 + 0.0978X_2 - 0.4513X_1X_2 + 0.7962X_1^2 + 0.1778X_2^2$
$k_6 = (0.0228 - 0.0001X_1 - 0.0019X_2) [\text{hr}^{-1}]$	$\alpha_6 = 1.1003 + 1.60X_1 - 0.5964X_2 + 0.1664X_1X_2 + 0.2152X_1^2 - 0.1765X_2^2$

RESULTS

Experiments were conducted to study the impact of *AR* and *SS* on the production of biomass, glucose and ethanol concentrations respectively. Generally, similar trends can be identified where there is increment in ethanol concentration and biomass concentration with the increase in *AR* and *SS*. On the other hand, glucose concentration decreased with the increase in *AR* and *SS*. These trends are generally identified with the increase in time. In each section below, the effect of *AR* and *SS* on each concentration is discussed.

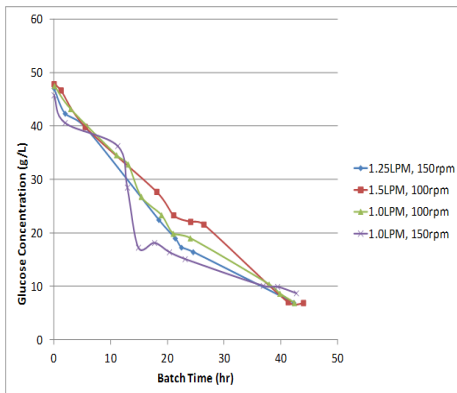


Fig.4: Graph of glucose concentration (g/L) vs. batch age (hr)

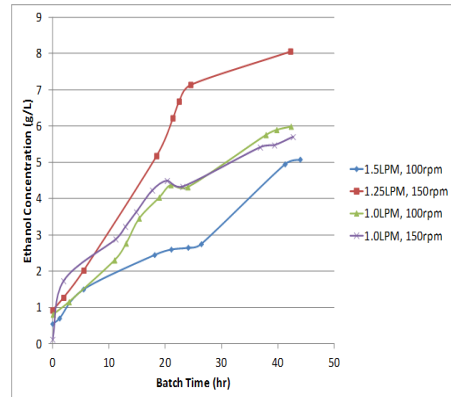


Fig.5: Graph of ethanol concentration (g/L) vs. batch age (hr).

Effect of Aeration Rate (AR) and Stirred Speed (SS) on Glucose Concentration

Fig.4 shows the trend of glucose concentration under different sets of *AR* and *SS*. As predicted, the glucose concentrations decreased with time under the influence of different sets of *AR* and *SS*. Glucose was consumed with time to produce ethanol. The rates of glucose consumption were quite comparable for all sets of *AR* and *SS*. This showed that although different conditions of *AR* and *SS* were implemented, the final glucose concentration attained was comparable. However, it is vital to investigate the amount of ethanol and biomass concentrations which can be produced under different *AR* and *SS* conditions since different amounts of glucose will be utilised to produce different amounts of ethanol and biomass concentrations.

Effect of Aeration Rate (AR) and Stirrer Speed (SS) on Ethanol Concentration

Fig.5 displays the ethanol concentration profiles under the influence of different *AR* and *SS* conditions. As predicted, as glucose concentration decreased, ethanol concentration increased with respect to time.

Generally, as observed from Fig.5, the ethanol concentration trend was not comparable under different conditions of *AR* and *SS* as compared to the glucose concentration trend from Fig.4. Notice that, when *AR* and *SS* was at 1.25 LPM and 150 rpm respectively (red line), ethanol concentration showed the highest value i.e. at 8.0 g/L. As observed from other *AR*

and *SS* conditions, the ethanol concentrations varied from 5.0 to 6.0 g/L, which were not significantly higher than 1.25 LPM *AR* and 150 rpm *SS*. These results show that although the glucose concentration trend was comparable, the ethanol concentration, however, varied under different conditions of *AR* and *SS*. Therefore, with the same amount of glucose concentration utilised, different amounts of ethanol concentration will be produced under different *AR* and *SS* conditions. Based on the ranges of *AR* and *SS* set for this study, the highest attainable ethanol concentration was at the mid-level range of *AR* i.e. 1.25 LPM, and the highest level range of *SS* i.e. at 150 rpm. The demands of the culture medium varied throughout the fermentation process, whereby the oxygen demand was low at the beginning of the process (Stanbury & Whitaker, 1995). However, due to high biomass content towards the end of the process, the oxygen demand was high. Therefore, it is inevitable that at *AR* of 1.25 LPM and *SS* of 150rpm, highest ethanol concentration was achieved. Although 1.25 LPM was not the highest level of *AR*, with the aid of *SS*, the highest ethanol concentration was produced at this level. These results show the importance of engaging both *AR* and *SS* in the production of ethanol.

Effect of Aeration Rate (AR) and Stirrer Speed (SS) on Biomass Concentration

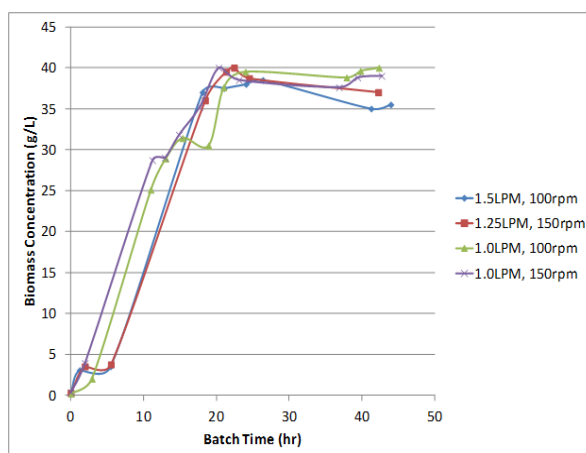


Fig.6: Graph of biomass concentration (g/L) vs. batch age (hr).

Fig.6 displays the variation of biomass concentration profile with different sets of *AR* and *SS*. As predicted, the biomass concentration increased with fermentation time. The rates of growth were comparable under different conditions of *AR* and *SS*. Compared to the trends of glucose and ethanol concentrations, glucose and biomass concentrations were comparable with fermentation time under different conditions of *AR* and *SS*. These observations showed that both glucose and biomass concentrations did not experience much variation within the *AR* and *SS* range. However, the ethanol concentration trend showed different variations with fermentation time.

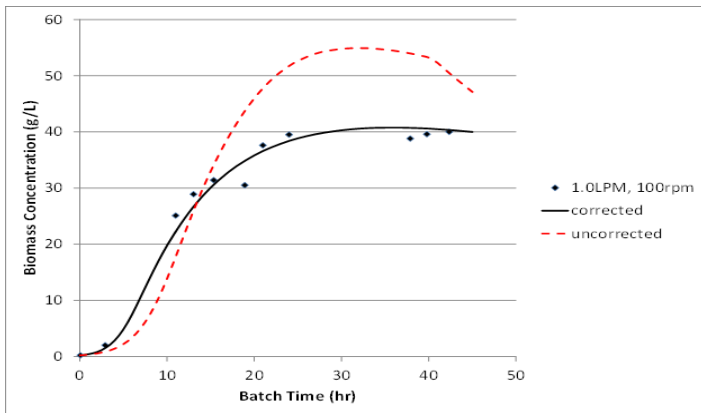
Based on studies done by Cot *et al.* (2007), the different amount of ethanol concentration was not likely due to the glucose and biomass concentrations produced. It was due to the cell viability with respect to the ethanol and biomass concentrations produced. During the fermentation process, the rate of ethanol concentration formation increased. Thus, the cell viability decreased. This phenomenon is due to the inhibition of ATP synthesis or leakage of metabolites from the cells while the yeast cells were metabolically inactive (Ghareib *et al.*, 1988). The plasma membrane was damaged and thus, the ethanol tolerance decreased. This caused the phospholipid content to decrease, which eventually caused cell death (Emily *et al.*, 2009). Due to this condition, different amounts of glucose were utilised to produce ethanol. Biomass concentration increased throughout the fermentation process and a vast proportion of biomass was produced towards the end of the fermentation process (Stanbury & Whitaker, 1995).

CFD Results

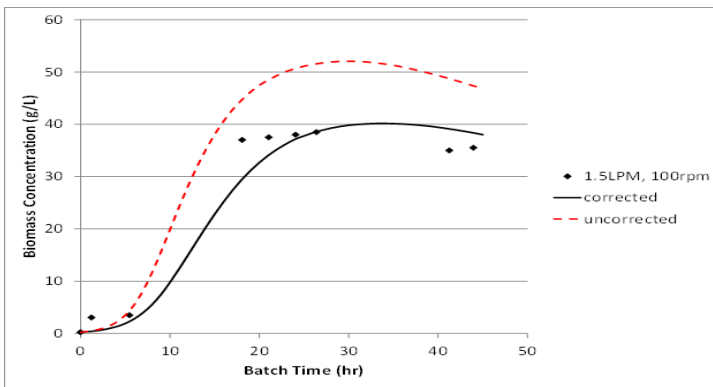
Validation of CFD simulation result. Table 3 gives the numerical values of the corrected kinetic parameters ($\alpha_i k_i$) and uncorrected kinetic parameters (k_i) for three different operating conditions. Simulations were carried out using these kinetic parameters and the accuracy of the models was compared with the experiment data.

TABLE 3 : Numerical Values of Corrected and Uncorrected Kinetic Parameters

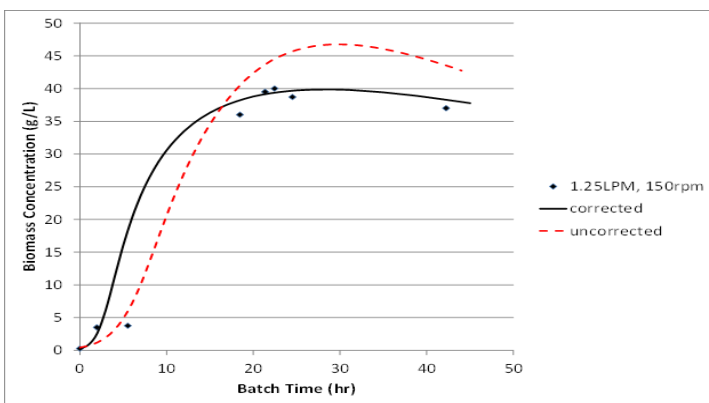
Parameters	Uncorrected values	Corrected values
AR = 1 LPM, SS = 100 rpm	$k_1 = 1.0697$	$k_{1,c} = 1.3373$
	$k_2 = 0.01$	$k_{2,c} = 0.01$
	$k_3 = 0.5158$	$k_{3,c} = 0.7736$
	$k_4 = 0.03827$	$k_{4,c} = 0.1148$
	$k_5 = 0.9443$	$k_{5,c} = 0.7743$
	$k_6 = 0.02607$	$k_{6,c} = 0.01294$
AR = 1.5 LPM, SS = 100 rpm	$k_1 = 0.9271$	$k_{1,c} = 0.65$
	$k_2 = 0.01$	$k_{2,c} = 0.01$
	$k_3 = 0.5084$	$k_{3,c} = 0.4072$
	$k_4 = 0.04537$	$k_{4,c} = 0.04553$
	$k_5 = 0.8933$	$k_{5,c} = 0.7079$
	$k_6 = 0.02602$	$k_{6,c} = 0.02593$
AR = 1.25 LPM, SS = 150 rpm	$k_1 = 1.25$	$k_{1,c} = 2.50$
	$k_2 = 0.01$	$k_{2,c} = 0.01$
	$k_3 = 0.5268$	$k_{3,c} = 1.16$
	$k_4 = 0.05035$	$k_{4,c} = 0.2517$
	$k_5 = 0.90473$	$k_{5,c} = 0.6633$
	$k_6 = 0.02478$	$k_{6,c} = 0.01402$



(a)



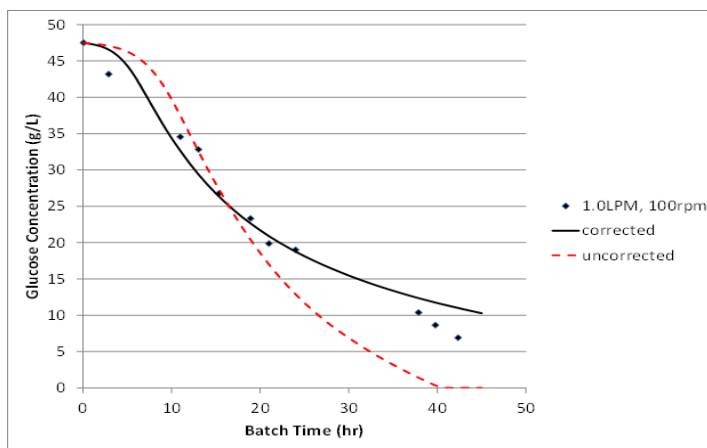
(b)



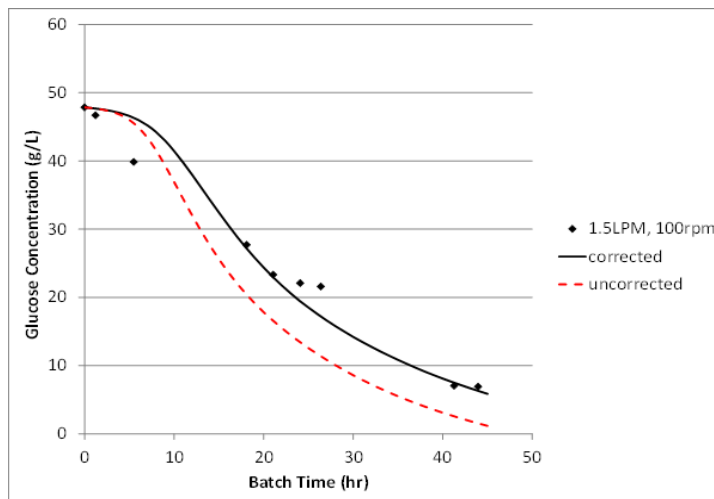
(c)

Fig.7: Prediction of biomass concentrations for (a) AR = 1.0 LPM and SS = 100 rpm; (b) AR = 1.5 LPM and SS = 100 rpm; (c) AR = 1.25 LPM and SS = 150 rpm using corrected and uncorrected kinetic parameters.

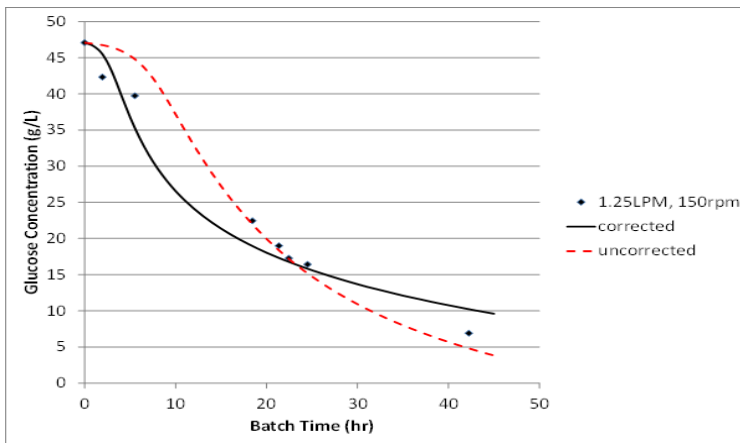
Figures 7 (a)-(c) show that the corrected kinetic model was able to predict the growth of biomass reasonably well compared to the uncorrected model for three different operating conditions. Generally, the biomass production was slow in the first few hours, e.g. batch time ≈ 4 hours for $AR = 1.0$ LPM and $SS = 100$ rpm. This is known as the lag phase, where the cells were adjusting to the medium (Rao, 2010). Then the biomass started to increase rapidly, up to batch time ≈ 20 hours. After that, the biomass content remained constant. The biomass was converted to ethanol during this process (Rao, 2010). Due to the shortage of the substrate (glucose), the biomass started to decrease. The biomass production was modelled using Monod-Herbert model, as shown in equation [9]. The growth rate was inhibited by the exponential term which was a function of ethanol concentration. The decay phase of the biomass was modelled as a linear function of biomass itself, which was significant at a high biomass concentration.



(a)



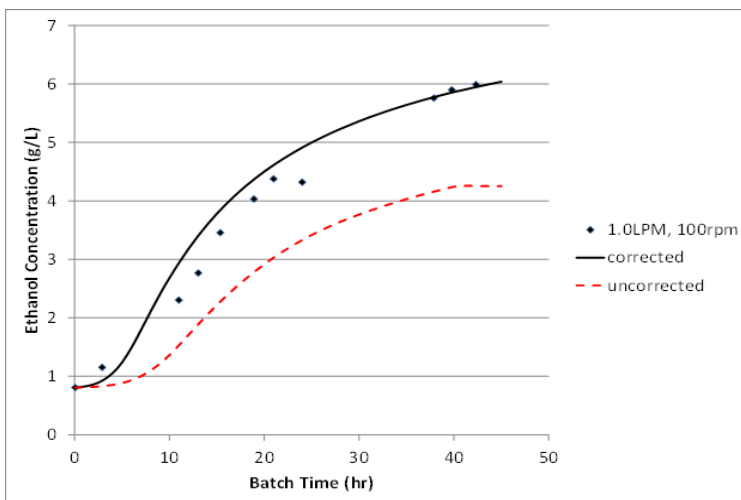
(b)



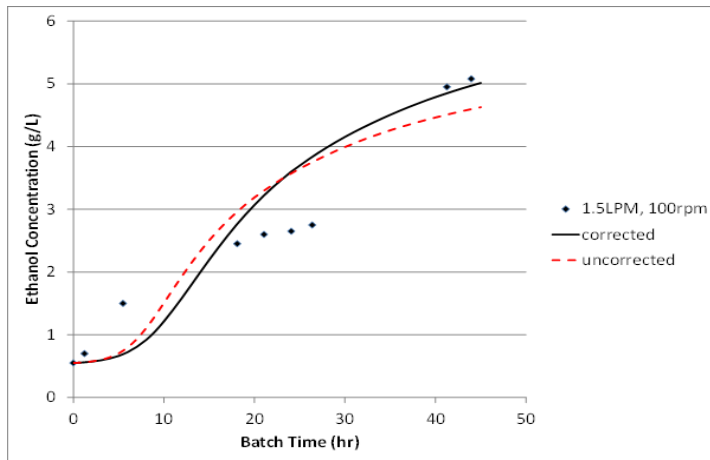
(c)

Fig.8: Prediction of glucose concentrations for (a) AR = 1.0 LPM, SS = 100 rpm; (b) AR = 1.5 LPM, SS = 100 rpm; (c) AR = 1.25 LPM, SS = 150 rpm using corrected and uncorrected kinetic parameters.

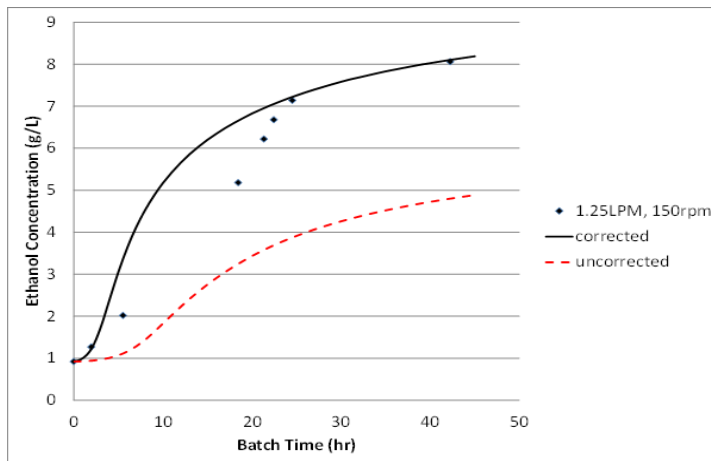
Fig.8 (a)-(c) show the simulated results of glucose consumption using the corrected and uncorrected kinetic parameters under different operating conditions. The experiment data was also shown. The results show that the uncorrected kinetics model predicted higher glucose consumption compared with the experiment findings. Similarly, the production of ethanol is assumed to be proportional to the growth of biomass; the uncorrected kinetic model underestimated the ethanol production as shown in Fig.9 (a)-(c). In both the glucose consumption and ethanol production models, the reaction rates were both inhibited at the higher ethanol concentration.



(a)



(b)

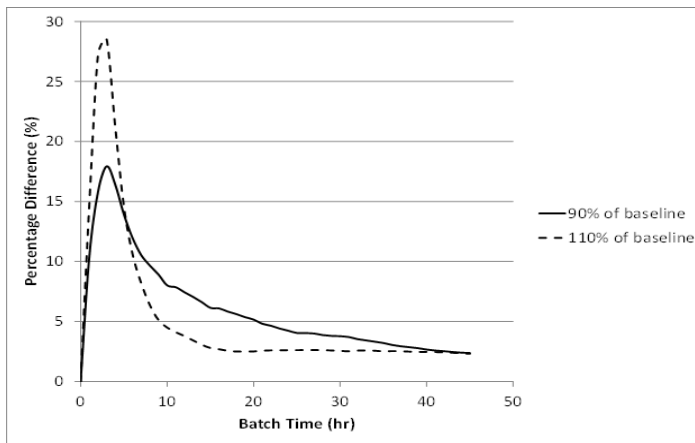


(c)

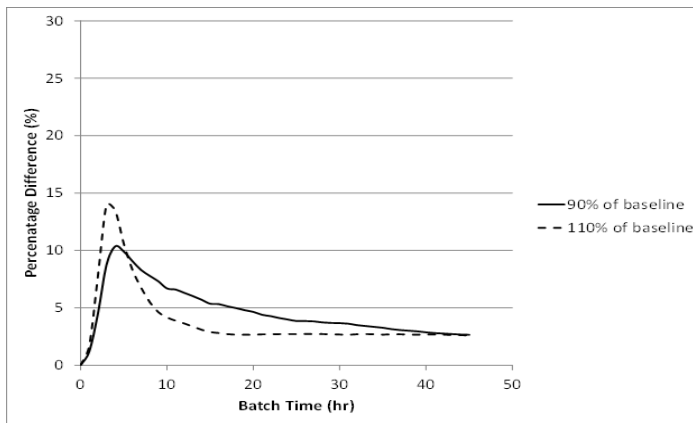
Fig.9: Prediction of ethanol concentrations for (a) AR = 1.0 LPM and SS = 100 rpm; (b) AR = 1.5 LPM and SS = 100 rpm; (c) AR = 1.25 LPM and SS = 150 rpm using corrected and uncorrected kinetic parameters.

Sensitivity Analysis of the Kinetic Parameters

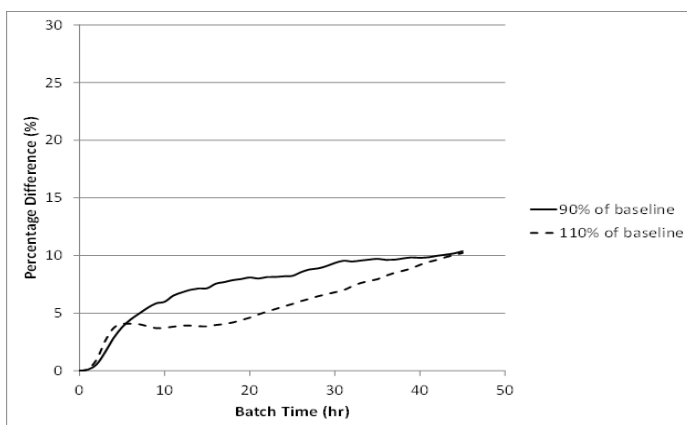
The fermentation kinetics model often requires a number of parameter estimations. There are six parameters in the current study i.e. k_1 to k_6 . To obtain the optimum values, it was important to carry out the sensitivity analysis of the parameter required. The analysis will reveal which parameters had a strong effect on the model results. Thus, the information was helpful in developing an optimisation algorithm for parameter estimation (Alcázar & Ancheyta, 2007). The sensitivity of the kinetic parameters, k_1 to k_6 on the biomass, ethanol and glucose was investigated for the case of AR = 1.25 LPM and SS = 150 rpm. This was treated as the baseline of the study. Each of the kinetic parameters was varied by $\pm 10\%$; the percentage differences of the material concentrations are presented in Fig.10 to Fig.15.



(a)



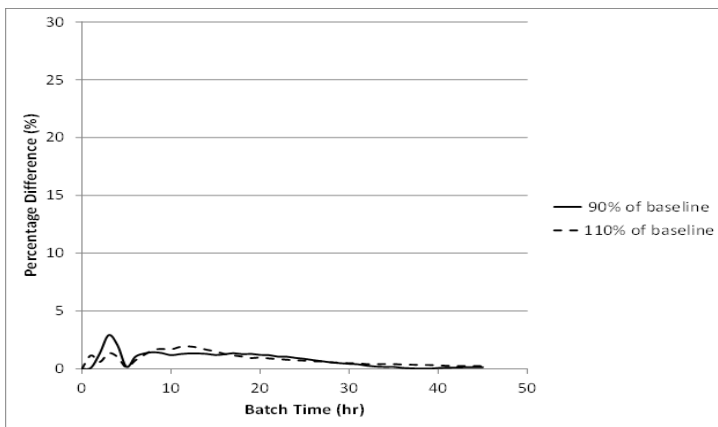
(b)



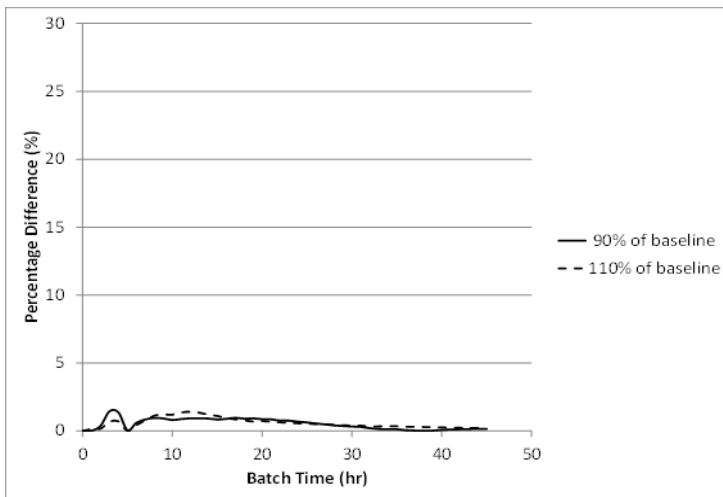
(c)

Fig.10: Percentage difference in the (a) production of biomass; (b) production of ethanol; (c) consumption of glucose, when the parameter, k_1 is changed by $\pm 10\%$.

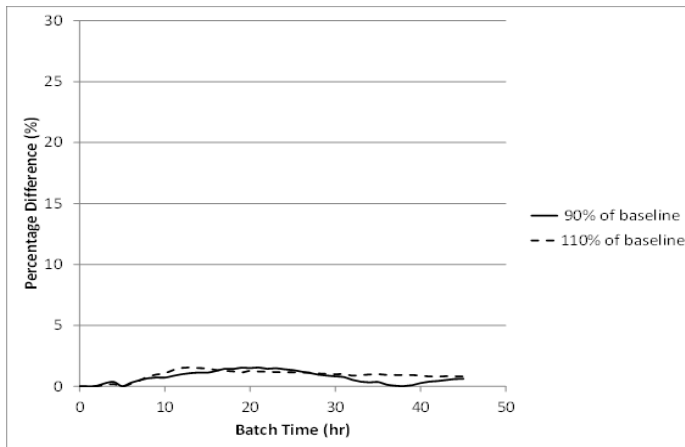
Fig.10 (a) shows that 10% variation in k_1 caused the biomass concentration difference to increase from zero to a maximum of 28%, after which, it decreased. The initial rapid increase was due to the biomass production and the availability of the high substrate (glucose) concentration. The rapid decrease of the percentage difference was caused by lower $(R_x)_{\text{growth}}$, which was due to the inhibition effect of the product (i.e. $\exp(-k_5 P) \frac{k_1 S X}{k_2 + S}$). Since biomass content was high as the batch time was longer, additional biomass produced did not cause a larger percentage difference. A similar trend was observed for the ethanol production as seen in Fig.10 (b). On the other hand, the percentage difference of the glucose increased with the batch time [Fig.10 (c)]. This was because although the glucose consumption rate was high at the initial stage, the availability of the glucose was high enough that the percentage difference was not significant. As the fermentation process proceeded, the glucose concentration was scarce and the percentage difference started to increase noticeably.



(a)



(b)

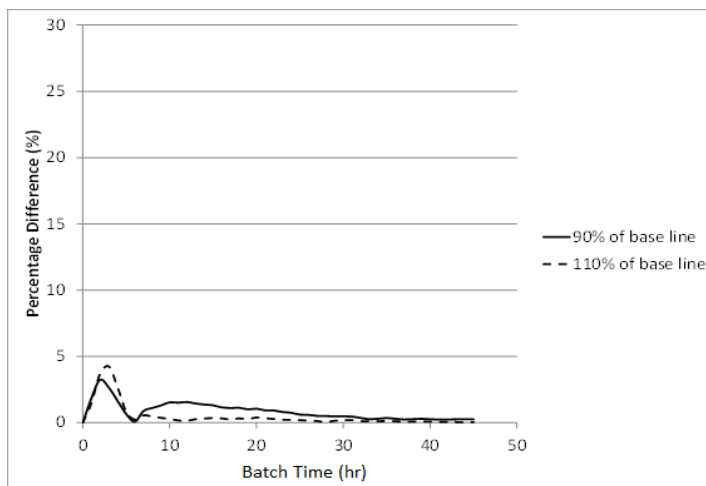


(c)

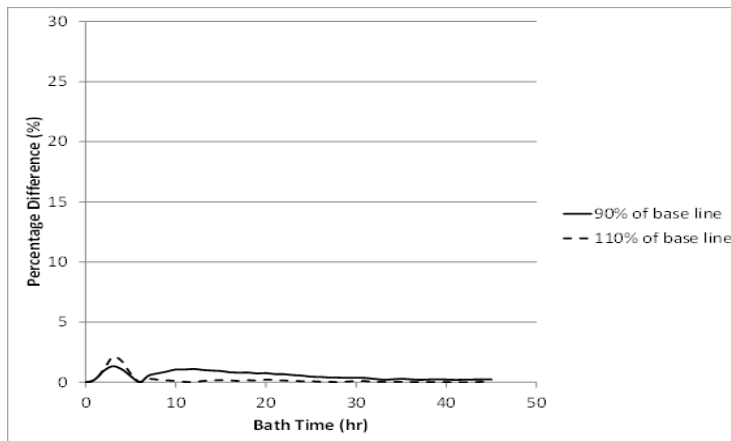
Fig.11: Percentage difference in the (a) production of biomass; (b) production of ethanol; (c) consumption of glucose, when the parameter, k_2 is changed by $\pm 10\%$.

The parameter k_2 did not have a significant effect on these three substances. Fig.11 (a)-(c) showed that the percentage differences were around 2-3% when k_2 was varied by 10%. This suggests that k_2 does not play an important role in optimum parameters estimation.

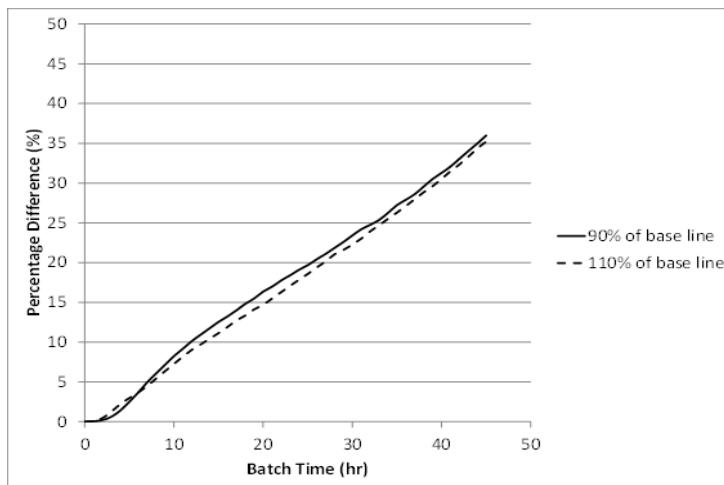
The parameter k_3 did not greatly affect the concentration of biomass and ethanol but it had a strong effect on the glucose utilisation as shown in Fig.12. Fig.12(c) indicates that the percentage difference of the glucose could be as high as 35% in the simulation, which is 3 times that of the k_3 variation.



(a)



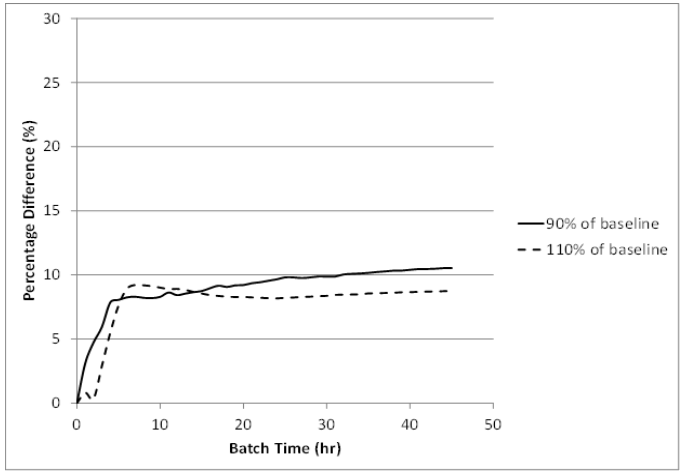
(b)



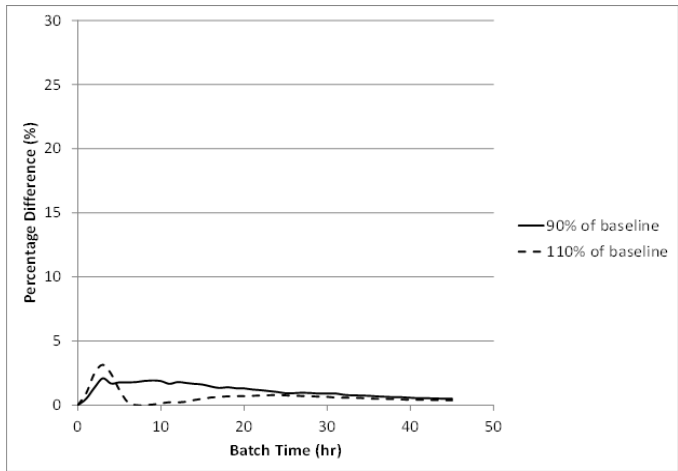
(c)

Fig.12: Percentage difference in the (a) production of biomass; (b) production of ethanol; (c) consumption of glucose, when the parameter, k_3 is changed by $\pm 10\%$.

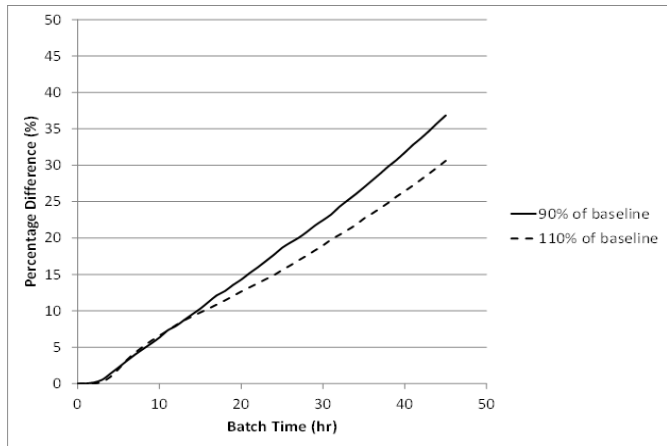
Fig.13 (a)-(c) reveal that parameter k_4 affected the biomass and glucose concentrations to a greater extent compared to ethanol concentration. The percentage difference for ethanol concentration was at most 3% compared to 10% and 36% for biomass and glucose concentrations, respectively. This is counter-intuition on hindsight because parameter k_4 was expected to affect ethanol more significantly compared to the others. Nevertheless, the observations are explained as follows: When parameter k_4 was varied, the variation in ethanol concentration was achieved, which in turn affected $(R_x)_{\text{growth}}$ in equation (6), as shown in Fig.13(d). $(R_x)_{\text{growth}}$ affected the biomass, ethanol and glucose concentrations as shown in equations (9)-(11). However, the reaction rate of the ethanol was much smaller (of the order of 10^{-5} kg/cm³s) compared to that of the biomass (of the order of 10^{-3} kg/m³s) and glucose (of the order of 10^{-4} kg/m³s). Thus, the ethanol concentration did not vary much when parameter was varied.



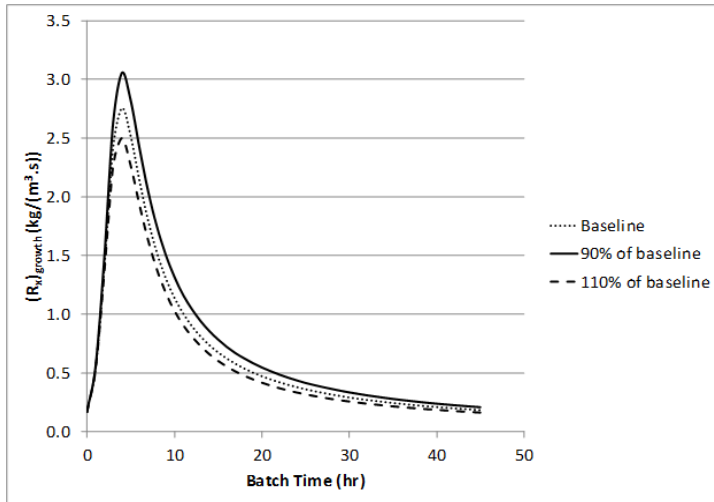
(a)



(b)



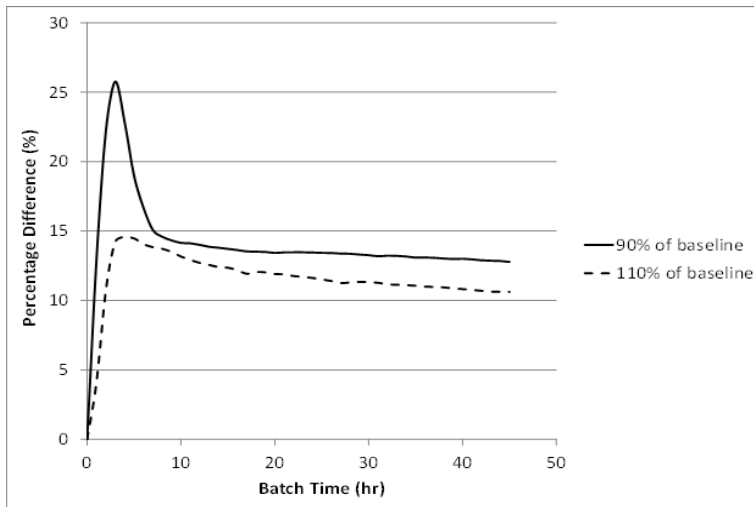
(c)



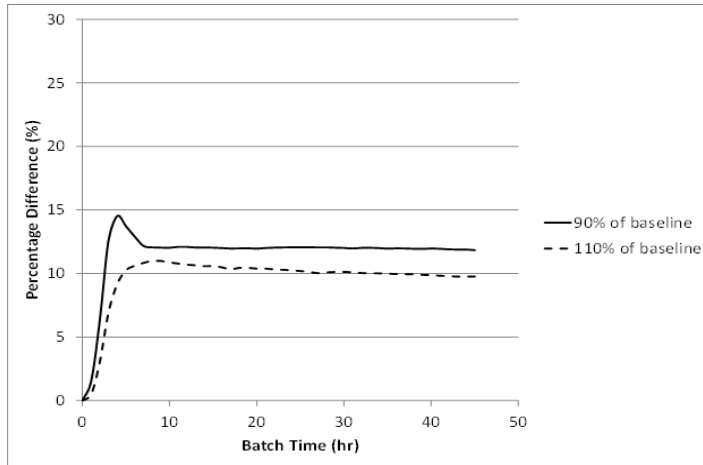
(d)

Fig.13: Percentage difference in the (a) production of biomass; (b) production of ethanol; (c) consumption of glucose; (d) $(R_x)_{\text{growth}}$ when the parameter, k_4 is changed by $\pm 10\%$.

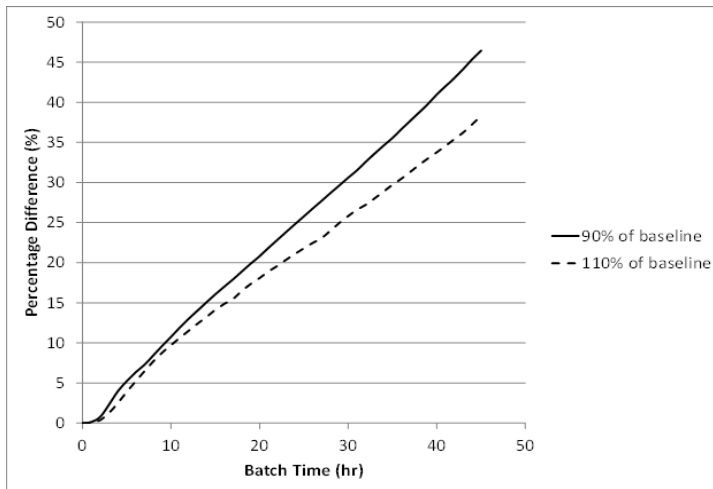
When the parameter, k_4 was varied, the maximum percentage difference for the biomass and ethanol concentrations was observed around batch time ≈ 4 hours, which corresponded to the maximum production rate [Fig.14 (a) - (b)]. On the other hand, the percentage difference of the glucose concentrations increased as shown in Fig.14(c).



(a)



(b)



(c)

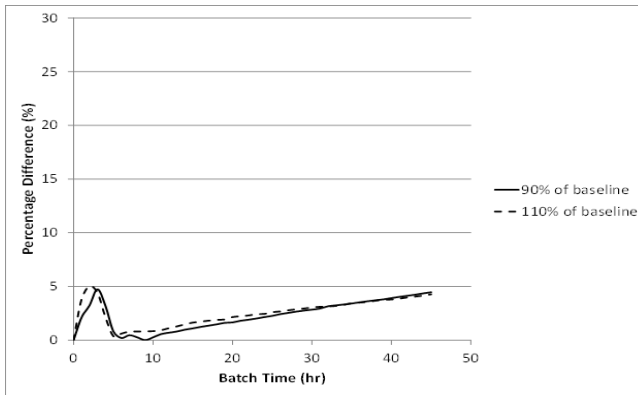
Fig.14: Percentage difference in the (a) production of biomass; (b) production of ethanol; (c) consumption of glucose, when the parameter, k_5 is changed by $\pm 10\%$.

Fig.15(a) shows the effects of parameter k_6 on biomass. It was observed that the effect was significant for biomass product. The percentage difference of the biomass increased since was related to biomass utilisation, as seen in equation (9). The ethanol and glucose concentrations were less affected by k_6 as shown in Figures 15 (b)-(c).

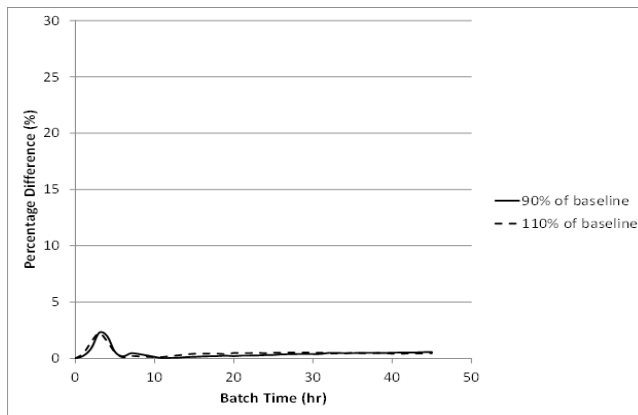
The sensitivity analysis showed that the fermentation process was most affected by (in the order of decreasing importance) k_5 , k_4 , k_3 , k_1 , k_6 and k_2 . This analysis is important as it aids CFD-based optimisation in future work.

The analysis above showed that the influence of each of the kinetic parameters varies with the concentration of biomass, glucose and ethanol, which are a function of the batch time.

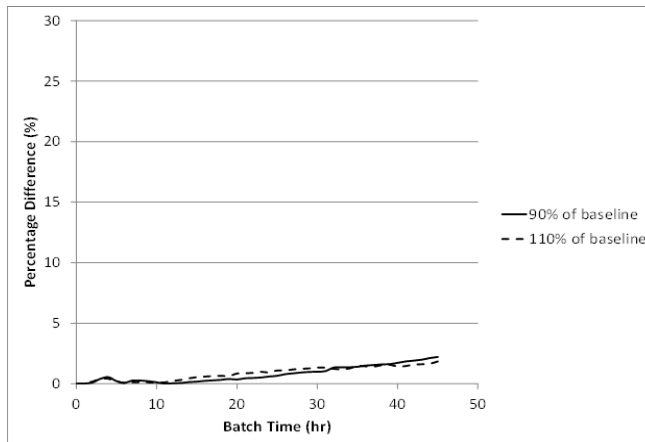
Simulation of a Bioreactor with an Improved Fermentation Model



(a)



(b)



(c)

Fig.15: Percentage difference in the (a) production of biomass; (b) production of ethanol; (c) consumption of glucose, when the parameter, k_6 is changed by $\pm 10\%$.

CONCLUSION AND FUTURE WORK

In this paper, a new kinetics model with the implementation of CFD simulation was proposed. The kinetic parameters of the ethanol fermentation based on Herbert's microbial kinetics, assuming perfectly-stirred condition, were not able to produce good predictions during CFD simulations. Correction factors based on a second-order spline were proposed to improve the CFD-based results. The coupled fermentation kinetics – CFD model is useful for practical purposes since the simulation time required is 2 hours to simulate a 45-hour fermentation process. A typical three dimensional two-phase flow fermentation kinetic-CFD model requires an approximate simulation time of 1 week. The work also highlights the need to incorporate a CFD model to obtain better kinetics parameter estimation. In this study, the maximum ethanol that can be produced was around 8.0 g/L, at the operating conditions of AR = 1.2 LPM and SS = 150 rpm. The corresponding kinetic parameters are: $k_{1,c} = 2.50$, $k_{2,c} = 0.01$, $k_{3,c} = 1.16$, $k_{4,c} = 0.2517$, $k_{5,c} = 0.6633$ and $k_{6,c} = 0.01402$. Future work is suggested to incorporate parameters such as temperature and pH into the improved kinetics model for further enhancement and improvement of the kinetics model.

REFERENCES

- Alcázar, L. A., & Ancheyta, J. (2007). Sensitivity analysis based methodology to estimate the best set of parameters for heterogeneous kinetic models. *Chemical Engineering Journal*, 128(2), 85-93.
- Bezzo, F., & Macchietto, S. (2004). A general methodology for hybrid multizonal/CFD models: Part II. Automatic zoning. *Computers & Chemical Engineering*, 28(4), 513-525.
- Cot, M., Loret, M., Francois, J., & Benbadis, L. (2007). Physiological behaviour of *Saccharomyces cerevisiae* in aerated fed-batch fermentation for high level production of bioethanol. *FEMS Yeast Research*, 7(1), 22-32.
- Elqotbi, M., Valev, S. D., Montastruc, L., & Nikov, I. (2013). CFD modelling of two-phase stirred bioreaction systems by segregated solution of the Euler-Euler model. *Computers and Chemical Engineering*, 48, 113-120.
- Emily, L. W. T., Nandong, J., & Samyudia, Y. (2009). Experimental investigation on the impact of aeration rate and stirrer speed on micro-aerobic batch fermentation. *Journal of Applied Sciences*, 9(17), 3126-3130.
- Fox, R. O., (1998). On the relationship between Lagrangian micromixing models and computational fluid dynamics. *Chemical Engineering and Processing: Process Intensification*, 37(6), 521-535.
- Garcia-Ochoa, F., & Gomez, E. (2009). Bioreactor scale-up and oxygen transfer rate in microbial processes: An overview. *Biotechnology Advances*, 27(2), 153-176.
- García-Ochoa, F., Santos, V. E., & Alcón, A. (1995). Xanthan gum production: An unstructured kinetic model. *Enzyme and Microbial Technology*, 17(3), 206-217.
- Ghareib, M., Youssef, K. A., & Khalil, A. A. (1988). Ethanol tolerance of *Saccharomyces cerevisiae* and its relationship to lipid content and composition. *Folia Microbiologica (Praha)*, 33(6), 447-452.
- Harvey, A. D., & Rogers, S. E. (1996). Steady and unsteady computation of impeller-stirred reactors. *AIChE Journal*, 42(10), 2701-2712.

- Hutmacher, D. W., & Singh, H. (2008). Computational fluid dynamics for improved bioreactor design and 3D culture. *Trends in Biotechnology*, 26(4), 166-172.
- Kuipers, J. A. M., & van Swaaij, W. P. M. (1998). Computational fluid dynamics applied to chemical reaction engineering. In F. Keil, W. Mackens, H. Voß, J. Werther (Eds.), *Scientific computing in chemical engineering ii: computational fluid dynamics, reaction engineering and molecular properties* (pP. 383-390). Berlin: Springer-Verlag.
- Kuzmin, D., Mierka, O., & Turek, S. (2007). On the Implementation of the k- turbulence model in incompressible flow solvers based in a finite element discretization. *International Journal of Computing Science and Mathematics*, 1, 193-206.
- Liew, E. W. T., Nandong, J., & Samyudia, Y. (2013). Multi-scale models for the optimization of batch bioreactors. *Chemical Engineering Sciences*, 95, 257-266.
- Patel, H., Ein-Mozaffari, F., & Dhib, R. (2010). CFD analysis of mixing in thermal polymerization of styrene. *Computers and Chemical Engineering*, 34(4), 421-429.
- Rao, D. G. (2010). *Introduction to biochemical engineering*. New Delhi: Tata McGraw Hill.
- Roudsari, S. F., Ein-Mozaffari, F., & Dhib, R. (2013). Use of CFD in modeling MMA solution polymerization in a CSTR. *Chemical Engineering Journal*, 219, 429-442.
- Schugerl, K., & Bellgardt, K. H. (2000). *Bioreaction engineering, modeling and control*. Springer-Verlag.
- Stanbury, P. F., Whitaker, A., & Hall, S. J. (1995). *Principles of fermentation technology*. Butterworth-Heinemann.
- Starzak, M., Kryzstek, L., Nowicki, L., & Michalski, H. (1994). Macroapproach kinetics of ethanol fermentation by *Saccharomyces cerevisiae*: Experimental studies and mathematical modelling. *The Chemical Engineering Journal and the Biochemical Engineering Journal*, 54(3), 221-240.
- Thatipamala, R., Rohani, S., & Hill, G. A. (1992). Effects of high product and substrate inhibitions on the kinetics and biomass and product yields during ethanol batch fermentation. *Biotechnology and Bioengineering*, 40(2), 289-297.
- Versteeg, H., & Malalasekera, W. (2007). *An introduction to computational fluid dynamics: The finite volume method*. Essex: Pearson.
- Van Zyl, J. M. (2012). *Three-dimensional modelling of simultaneous saccharification and fermentation of cellulose to ethanol* (Doctoral dissertation). Stellenbosch: Stellenbosch University.